International Journal of Heat and Mass Transfer 119 (2018) 533–541

Contents lists available at ScienceDirect

International Journal of Heat and Mass Transfer

journal homepage: www.elsevier.com/locate/ijhmt

A mesh-free Monte-Carlo method for simulation of three-dimensional transient heat conduction in a composite layered material with temperature dependent thermal properties

Reza Bahadori [a,*], Hector Gutierrez [a], Shashikant Manikonda [b], Rainer Meinke [b]

[a] The Florida Institute of Technology, Melbourne, FL 32901, USA
[b] The AML Superconductivity and Magnetics, Palm Bay, FL 32905, USA

ARTICLE INFO

Article history:
Received 20 September 2017
Received in revised form 7 November 2017
Accepted 28 November 2017

Keywords:
Monte-Carlo methods
Conductive heat transfer
Composite materials
Mesh-free methods
Non-homogeneous materials
Thermal diffusivity
Finite element methods

ABSTRACT

A new solution for the three-dimensional transient heat conduction from a homogeneous medium to a non-homogeneous multi-layered composite material with temperature dependent thermal properties using a mesh-free Monte-Carlo method is proposed. The novel contributions include a new algorithm to account for the impact of thermal diffusivities from source to sink in the calculation of the particles' step length (particles are represented as bundles of energy emitted from each source), and a derivation of the three-dimensional peripheral integration to account for the influence of material properties around the sink on its temperature. Simulations developed using the proposed method are compared against both experimental measurements and results from a finite element simulation.

1. Introduction

The Monte-Carlo method (MCM) is prominent for its ability to tackle complex simulation problems based on random number generation. Numerical solutions based on finite difference and finite element methods have been conventionally adopted for solving multi-dimensional heat conduction problems, although some issues remain problematic with these approaches. For instance, the stability criterion in the explicit finite difference method limits the time step to the grid size. Implicit approaches [1] are used in the majority of linear solvers and FEM packages due to their numerical stability. Implicit applications convert the problem's geometry to a grid of small elements that lead to a matrix that must be solved by inversion to obtain the result at each time increment. Complex geometries that require small grid size lead to large matrices and therefore larger computational and memory requirements: inversion of large assembly matrices is time consuming. This becomes a significant practical consideration in problems with complex geometries and Multiphysics problems [2]. By contrast, Monte-Carlo methods have significant advantages relative to these methods [3]. First, there is no requirement to build an assembly matrix and consequently no need for matrix inversion. Second, the solution at a desired point in the domain can be obtained independently from the solutions at other points within the domain. These features lead to a significant reduction in simulation time by solving for specific regions of interest, instead of solving for the entire domain, which requires inversion of the entire assembly matrix. Inverse heat conduction (the prediction of surface temperature and heat flux using the time history of temperature at internal points in the domain) is another important problem that benefits from this feature [4]. Third, the Monte-Carlo approach is stable and very well suited for parallel computing, which is particularly attractive with the advent of GPU engines [2]. Apart from the aforementioned general advantages, using random parameters in MCM makes it a powerful approach to model problems with inherited random or stochastic behaviors or parameters. For instance porosity in porous media can be defined as a random parameter [5–9], making MCM an excellent option for simulation.

The Monte-Carlo method was first described in 1949 [10] by Metropolis and Ulam as a statistical approach for solving integro-differential equations. In heat conduction, Haji-Sheikh and Sparrow [11] described the application of MCM to solve heat

* Corresponding author.
E-mail addresses: rbahadori2013@my.fit.edu (R. Bahadori), hgutier@fit.edu (H. Gutierrez), smanikonda@amlsm.com (S. Manikonda), rbmeinke@amlsm.com (R. Meinke).

https://doi.org/10.1016/j.ijheatmasstransfer.2017.11.140
0017-9310/

conduction problems with homogenous isotropic material properties for different types of boundary conditions. Other studies have used [11] to develop methods to solve conduction heat transfer problems where thermal properties are not isotropic, as in composite layered materials. The fixed random walk MCM was modified [12,13] to solve transient heat conduction in anisotropic media. The necessity of a grid to define the geometry is a disadvantage of the fixed random walk method, compared to floating random walk. Non-homogeneity of thermal properties in a heat conduction domain has been shown in [14] by relating the impact of the non-homogeneity on the temperature distribution in proportion to the thermal diffusivity of source and sink. In cases with abrupt changes in thermal diffusivity, such as at cryogenic temperatures or in composite layered materials, the aforementioned approach of proportion leads to significant error. This paper presents a novel solution for transient heat conduction in anisotropic materials with abrupt changes in thermal diffusivity based on MCM.

2. Formulation

Heat transfer process describes the transmission of an energy bundle (particle in this study) from source to sink. In a reverse approach, one can use the known thermal properties of the sink to estimate the sources that can transfer energy to the sink in a corresponding time span. The domain is filled with K uniformly generated points that represent sinks with known initial conditions that define the temperature at each point. The solution process starts by emitting J particles from each sink to find the location of the sources, which could be anywhere within or beyond the boundaries of the domain and not necessarily on the sink locations. If the source location falls inside the domain, the temperature at that location can be interpolated using the known temperatures of neighboring points from the previous time step. The scattered interpolation uses four closest neighboring points. Otherwise, the following boundary conditions apply for particles falling on or outside of boundaries at each time step. First, a fixed temperature boundary condition: particles adopt the pre-assigned fixed temperature of the boundary. Second: Insulation boundary condition: particles adopt the temperature of the sink. Third: convection boundary condition, has not been considered in this paper. Other studies [15,16] have proposed methods for taking the convective boundary condition into account. Three-dimensional conductive heat transfer in a domain with homogeneous thermal diffusivity (as described in [11]) presents the method to estimate source locations. From the three dimensional heat conduction relation in spherical coordinates ([17,18]) one can find the temperature at the sphere's center as:

$$T(x,y,z,t) = \int_{F=0}^{1}\int_{G=0}^{1}\int_{\tau=0}^{t} T(r,\varphi,\theta,t-\tau)dFdGdH^{(3)} \tag{1}$$

$$F(\varphi) = \frac{\varphi}{2\pi} \tag{2}$$

$$G(\theta) = \frac{1}{2}(1-cos\theta) \tag{3}$$

$$H^{(3)}\left(\frac{\alpha\tau}{r^2}\right) = 1 + 2\sum_{k=1}^{\infty}(-1)^k \exp\left(\frac{-k^2\pi^2\alpha\tau}{r^2}\right) \tag{4}$$

Eq. (1) illustrates the integral form for the temperature at the sphere's center based on the known temperature of particles emitted from its vicinity. Eqs. (2) and (3) describe the probability functions of angles θ and φ, respectively. The time step τ and steplength r of each floating random walk are related to the thermal diffusivity α at each point by the probability function (4): the higher the thermal diffusivity, the longer the step length (or the shorter the required time step). The inverse functions for Eqs. (2)–(4) [19] are: Eq. (7) is obtained from a fit function on inverse of Eq. (4).

$$\varphi = 2\pi(RN_1) \tag{5}$$

$$\theta = cos^{-1}[1-2(RN_2)] \tag{6}$$

$$\begin{aligned} \frac{\alpha\tau}{r^2} &= D_1 + D_2(RN_3) + D_3(RN_3)^2 + D_4(RN_3)^3 \quad RN3 < 0.6 \\ \frac{\alpha\tau}{r^2} &= -0.10132ln[0.5(1-RN_3)] \quad RN3 \geqslant 0.6 \end{aligned} \tag{7}$$

RN in Eqs. (5)–(7) denotes uniform random numbers generated from a Halton sequence (uniformly distributed random numbers) in three different sets. Table 1 shows the values of the D coefficients in these equations [19].

Fig. 1 depicts the inverse of the probability function $H^{(3)}$, where the random number RN_3 from the Halton sequence is the abscissa and the ordinate value is $\frac{\alpha\tau}{r^2}$. With the known thermal diffusivity of sink α and time step τ, the steplength r can be calculated.

By calculating the angles and steplength as described above, one can calculate the location of the source using Eq. (8). Once the source location is defined, the temperature at that location is allocated to the particle emitted from the respective source. The sink's temperature is simply the average of the temperature of particles as shown in Eq. (9), where j is the index for the particle number of J particles, t the time step and k the index for point number out of a total of K points [11]:

$$\begin{aligned} x_j &= x_k + r_j\sin(\theta_j)\cos(\varphi_j) \\ y_j &= y_k + r_j\sin(\theta_j)\sin(\varphi_j) \\ z_j &= z_k + r_j\sin(\theta_j) \end{aligned} \tag{8}$$

$$T^{t+1}_{(x_k,y_k)} = \frac{1}{J}\sum_{j=1}^{J} T^{t}_{(x_j,y_j)} \tag{9}$$

Fig. 2 depicts $J = 20$ particles emitted from the source and absorbed by the sink at the center of the sphere. The location of the sources is calculated using the aforementioned approach.

The above equations cover the solution of diffusion problems in homogenous media. Tackling problems in non-homogenous media needs further modifications. First, the thermal diffusivity of and between the source and the sink are not equal; therefore, the steplength calculated from the sink using its thermal diffusivity will not be equal to the steplength calculated from the source using its diffusivity. This affects the reversibility of the particle transport described before: reversibility is not valid in non-homogenous media.

A new algorithm is needed that takes into account the change in thermal diffusivity between source and sink. One approach is to take very small time steps, leading to steplengths small enough to approximate the thermal diffusivity of source and sink as equal. This has some disadvantages: assuming equal thermal diffusivity introduces error, and the approximation is not applicable close to the boundaries in composite layered materials, where thermal diffusivity experiences an abrupt change. Also, acquiring results for desired times requires more iterations due to the smaller time steps, which increases simulation time.

Knowing the thermal diffusivity function enables methods to address the aforementioned issue for non-homogenous media [20,21]; however this may lead to error in case of sharp changes in diffusivity due to the use of derivatives. Refs. [22] shows the required modifications to the two-dimensional Monte-Carlo transient heat conduction equations in cylindrical coordinates that lead

Table 1
Coefficients of the inverse probability function.

RN_3	D_1	D_2	D_3	D_4
0.0–0.1	0.079578	0.079621	0.058919	0.048997
0.1–0.3	0.079515	0.081077	0.048261	0.074542
0.3–0.6	0.070722	0.150740	−0.13699	0.240830

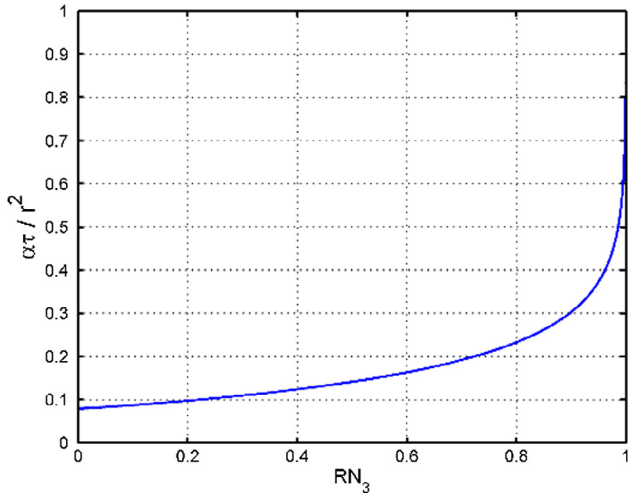

Fig. 1. Inverse function of the probability function $H^{(3)}$.

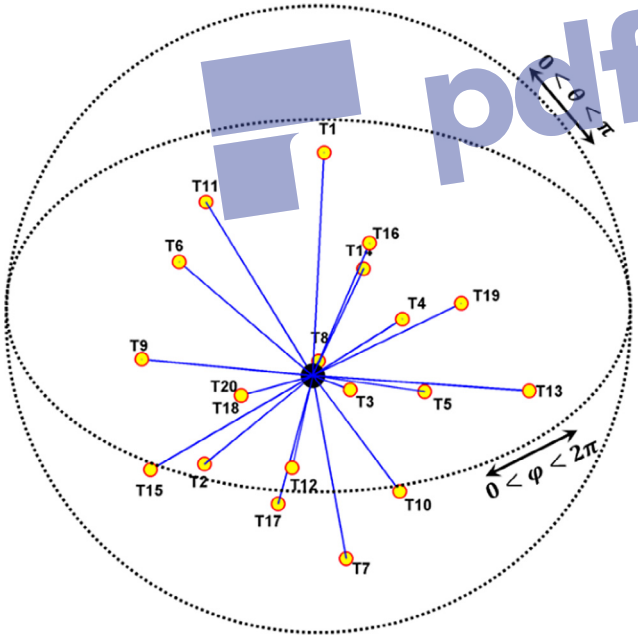

Fig. 2. Variables affecting T_C, before modification of Eq. (9).

to a method that works for non-homogenous and multilayered composite domains. This paper presents the required modifications for the three-dimensional case in spherical coordinates. The inverse of the probability distribution function $H^{(3)}$ can be obtained from Eqs. (5)–(7) and expressed as C:

$$\frac{\alpha\tau}{r^2} = C \tag{10}$$

The steplength r can then be calculated as:

$$r = \sqrt{\frac{\alpha\tau}{C}} \tag{11}$$

In the proposed algorithm, the steplength r is divided in M smaller steplengths, and the thermal diffusivity is updated at each new location:

$$r_j = \sum_{m=1}^{M} r_m = \sum_{m=1}^{M} \sqrt{\frac{\alpha_m \tau}{CM^2}} \tag{12}$$

where index $1 \leqslant m \leqslant M$ denotes the location of the jth particle after passing each sub-steplength:

$$\begin{aligned} x_{m+1} &= x_m + r_m \sin(\theta_j)\cos(\varphi_j) \\ y_{m+1} &= y_m + r_m \sin(\theta_j)\sin(\varphi_j) \\ z_{jm+1} &= z_m + r_m \cos(\theta_j) \end{aligned} \tag{13}$$

At the beginning of the process, the location of the kth point is: $m = 1$, $x_1 = x_k$, $y_1 = y_k$ and $z_1 = z_k$. In the next step, the jth particle is emitted from point k along the direction generated by angles θ_j and φ_j with sub-steplength r_j calculated from Eq. (12). New locations x_2, y_2 and z_2 are calculated using Eq. (13) and the thermal diffusivity at the new location is used to calculate the next sub-steplength – this process is repeated for M iterations. M can be adjusted for each part of the domain separately; it can be larger for regions with larger variations in thermal diffusivity (or with thin layers of composite materials) or can be smaller for regions with smooth changes in thermal diffusivity within one material. The adjustability of M enables adjusting the solution within the domain to achieve a desired accuracy in reasonable simulation time. This modification not only corrects the size of the steplength but also provides information for the next modification: the calculation of temperature at each point using peripheral integration.

A modified Bessel function method relates the time step and steplength in a transient solution, and gives the particles' temperature, location and thermal diffusivity at each sub-steplength around each point in the solution. This information is then used to find the temperature at each point. The next modification requires derivation of the steady state heat conduction equation in spherical coordinates to define the temperature at the center of the sphere based on the temperature of the particles in its vicinity forming a spherical region. The steady state heat diffusion in spherical coordinates is:

$$\begin{aligned} &\frac{1}{r^2 sin^2(\theta)}\frac{\partial}{\partial\varphi}\left(k(r,\theta,\varphi)\frac{\partial T(r,\theta,\varphi)}{\partial\varphi}\right) \\ &+\frac{1}{r^2 sin(\theta)}\frac{\partial}{\partial\theta}\left(k(r,\theta,\varphi)\sin(\theta)\frac{\partial T(r,\theta,\varphi)}{\partial\varphi}\right) \\ &+\frac{1}{r^2}\frac{\partial}{\partial r}\left(k(r,\theta,\varphi)r^2\frac{\partial T(r,\theta,\varphi)}{\partial r}\right) = 0 \end{aligned} \tag{14}$$

By integration of (14) with respect to φ from 0 to 2π, the first expression becomes zero due to having the same conditions at the beginning and end of the traverse:

$$\begin{aligned} &\int_0^{2\pi}\frac{1}{r^2 sin^2(\theta)}\frac{\partial}{\partial\varphi}\left(k(r,\theta,\varphi)\frac{\partial T(r,\theta,\varphi)}{\partial\varphi}\right)d\varphi \\ &=\frac{1}{r^2 sin^2(\theta)}\left(k(r,\theta,2\pi)\frac{\partial T(r,\theta,2\pi)}{\partial\varphi}-k(r,\theta,0)\frac{\partial T(r,\theta,0)}{\partial\varphi}\right)=0 \end{aligned} \tag{15}$$

Multiplying both sides of the remaining terms of Eq. (14) by $sin(\theta)$ and integrating from 0 to π with respect to θ makes the second term in Eq. (14) equal to zero as well, since:

$$\int_0^{2\pi}\left(k(r,\pi,\varphi)\sin(\pi)\frac{\partial T(r,\pi,\varphi)}{\partial\varphi}-k(r,\pi,\varphi)sin(0)\frac{\partial T(r,0,\varphi)}{\partial\varphi}\right)d\varphi=0 \tag{16}$$

From this it follows:

$$\int_0^{2\pi}\int_0^{\pi}\sin(\theta)\frac{\partial}{\partial r}\left(k(r,\theta,\varphi)r^2\frac{\partial T(r,\theta,\varphi)}{\partial r}\right)d\theta d\varphi = 0 \tag{17}$$

Finally, integration with respect to r from 0 to r yields

$$\int_0^{2\pi}\int_0^{\pi}\sin(\theta)r^2k(r,\theta,\varphi)\frac{\partial T(r,\theta,\varphi)}{\partial r}d\theta d\varphi = 0 \tag{18}$$

Burmeister [23] presented a similar derivation in two-dimensional cylindrical coordinates for the steady state condition – consequently, after integration, r results to be a constant. In our derivation (Eq. (18)) r^2 is not considered constant even though the derivation is for steady-state. Time and steplength in the previous modification are obtained from the modified Bessel function solution, so each particle has a different steplength, r. Hence, it cannot come out in the integration of (18). The following coordinate transformation is proposed:

$$\eta = \frac{\int_0^r \frac{dr'}{k(r',\theta,\varphi)r^2\sin(\theta)}}{\int_0^R \frac{dr'}{k(r',\theta,\varphi)r^2\sin(\theta)}} \tag{19}$$

$$f = \frac{\int_0^{\theta}\frac{d\theta'}{\int_0^R \frac{dr'}{k(r',\theta',\varphi)r^2\sin(\theta)}}}{\int_0^{\pi}\frac{d\theta'}{\int_0^R \frac{dr'}{k(r',\theta',\varphi)r^2\sin(\theta)}}} \tag{20}$$

$$g = \frac{\int_0^{\varphi}\int_0^{\pi}\frac{d\theta' d\varphi'}{\int_0^R \frac{dr'}{k(r',\theta',\varphi')r^2\sin(\theta)}}}{\int_0^{2\pi}\int_0^{\pi}\frac{d\theta' d\varphi'}{\int_0^R \frac{dr'}{k(r',\theta',\varphi')r^2\sin(\theta)}}} \tag{21}$$

This transformation aims at defining $T(r,\theta,\varphi)$ in terms of $T(\eta,f,g)$. Therefore, it satisfies the total differential relationship:

$$\begin{aligned} &dT(r,\theta,\varphi) = dT(\eta,f,g) \Rightarrow \\ &\frac{\partial T(r,\theta,\varphi)}{\partial r}dr + \frac{\partial T(r,\theta,\varphi)}{\partial \theta}d\theta + \frac{\partial T(r,\theta,\varphi)}{\partial \varphi}d\varphi = \\ &\frac{\partial T(\eta,f,g)}{\partial \eta}d\eta + \frac{\partial T(\eta,f,g)}{\partial f}df + \frac{\partial T(\eta,f,g)}{\partial g}dg \end{aligned} \tag{22}$$

This implies:

$$\frac{\partial T(r,\theta,\varphi)}{\partial r}dr = \frac{\partial T(\eta,f,g)}{\partial \eta}d\eta \tag{23}$$

Using Eq. (19), $d\eta$ can be expressed as shown below, where A and I_RA are defined to simplify its representation in the next steps:

$$d\eta = \frac{\frac{dr}{k(r,\theta,\varphi)r^2\sin(\theta)}}{\int_0^R \frac{dr'}{k(r',\theta,\varphi)r^2\sin(\theta)}} = \frac{A}{I_RA}dr \tag{24}$$

The term $\frac{\partial T(r,\theta,\varphi)}{\partial r}$ in Eq. (18) can be written as:

$$\frac{\partial T(r,\theta,\varphi)}{\partial r} = \frac{\partial T(\eta,f,g)}{\partial \eta}\frac{A}{I_RA} \tag{25}$$

The remaining terms in Eq. (18) can be defined as:

$$\begin{aligned} df &= \frac{\frac{d\theta}{\int_0^R \frac{dr'}{k(r',\theta,\varphi)r^2\sin(\theta)}}}{\int_0^{\pi}\frac{d\theta'}{\int_0^R \frac{dr'}{k(r',\theta',\varphi)r^2\sin(\theta)}}} = \frac{B}{I_\pi B}d\theta \\ &\Rightarrow d\theta = \frac{I_\pi B}{B}df \end{aligned} \tag{26}$$

$$dg = \frac{\int_0^{\pi}\frac{d\theta' d\varphi}{\int_0^R \frac{dr'}{k(r',\theta',\varphi)r^2\sin(\theta)}}}{\int_0^{2\pi}\int_0^{\pi}\frac{d\theta' d\varphi'}{\int_0^R \frac{dr'}{k(r',\theta',\varphi')r^2\sin(\theta)}}} = \frac{E}{I_{2\pi}E}d\varphi \Rightarrow d\varphi = \frac{I_{2\pi}E}{E}dg \tag{27}$$

Substituting Eqs. (25)-(27) in Eq. (18) yields:

$$\int_0^{2\pi}\int_0^{\pi}\frac{1}{A}\frac{\partial T(\eta,f,g)}{\partial \eta}\frac{A}{I_RA}\frac{I_\pi B}{B}\frac{I_{2\pi}E}{E}dfdg = 0 \tag{28}$$

Note that $\sin(\theta)r^2k(r,\theta,\varphi) = \frac{1}{A}$, $I_RA = \frac{1}{B}$, $I_\pi B = E$, $I_{2\pi}E = Constant$. Eq. (18) can then be written after the proposed transformation as:

$$\int_0^1\int_0^1\frac{\partial T(\eta,f,g)}{\partial \eta}dfdg = 0 \tag{29}$$

To define the temperature at the center in terms of the specified peripheral temperatures, integration with respect to η from 0 to the outer radius of each particle is performed. T_c represents the temperature at the center ($\eta = 0$) and T_R the specified peripheral temperatures for $\eta = 1$:

$$\int_0^1\int_0^1(T_R - T_C)dfdg = 0 \tag{30}$$

Substituting df and dg in Eq. (30) using the thermal diffusivity, α, instead of the thermal conductivity, k, the center temperature for the transient case is:

$$T_C = \frac{\int_0^{2\pi}\int_0^{\pi}\frac{\sin(\theta)r^2T(R,\theta,\varphi)}{\int_0^R\frac{dr'}{\alpha(r',\theta,\varphi)}}d\theta d\varphi}{\int_0^{2\pi}\int_0^{\pi}\frac{r^2\sin(\theta)}{\int_0^R\frac{dr'}{\alpha(r',\theta,\varphi)}}d\theta d\varphi} \tag{31}$$

For each particle at angles θ and φ, the radius r is a known constant value and can come out of the most internal integration. Eq. (31) and its variables are represented in Fig. 4. Comparison with Fig. 2 shows the effect of the proposed modifications on the calculation of each point's temperature. Fig. 3 shows each particles' steplength divided in M sub-steplengths using Eq. (12) with $M = 4$. Eq. (12) is applied to all particles' steplength in Fig. 4, but for clarity, sub-steplengths are shown for one steplength only. Compared to Eq. (9), Eq. (31) is suitable for multilayered composite structures with temperature dependent thermal properties. However, it is general form and if material properties are constant in whole domain, Eq. (31) can be simplified to Eq. (9).

Fig. 4 shows the spherical geometry around point k made by the total number of particles $J = 20$. Clearly, having more particles allows finer representation of the volume around the sink, leading to a more accurate simulation of the temperature distribution. The

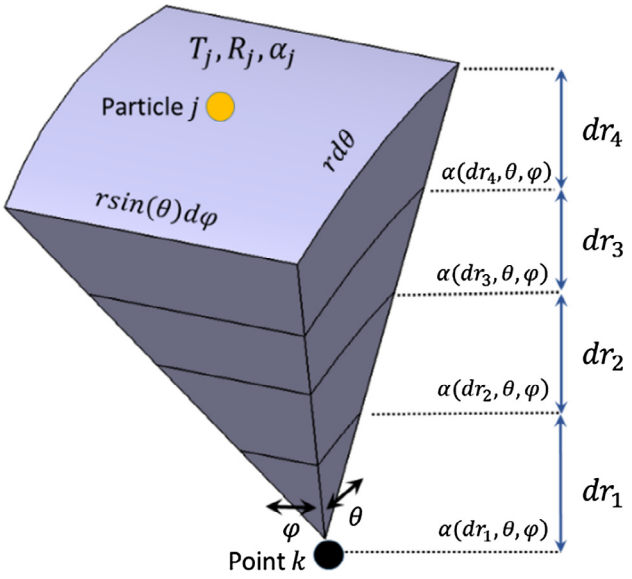

Fig. 3. Variables participating in T_C after proposed modification, Eq. (31), shown only for one particle.

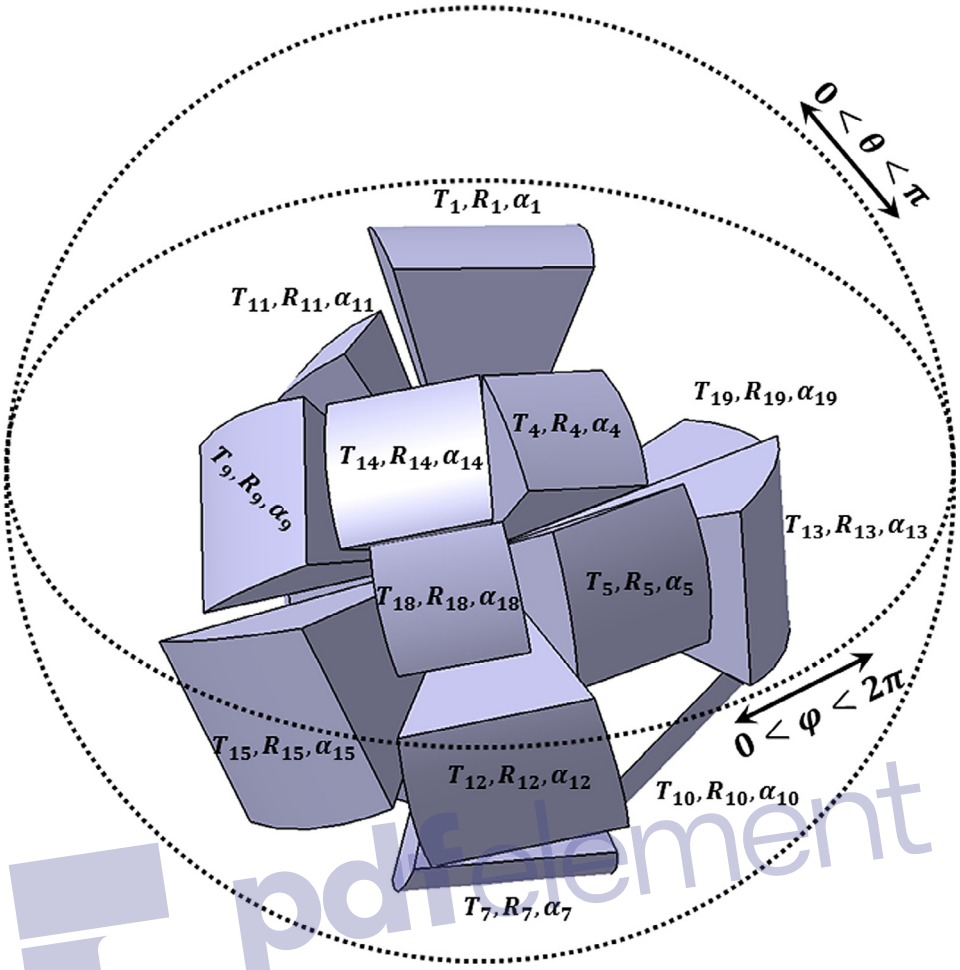

Fig. 4. Variables participating in T_C after proposed modification, Eq. (31).

square pyramidal shapes shown in Figs. 3 and 4 are not representing grid elements as known in methods such as FEM – they are just a schematic representation of the variables in Eq. (31).

3. Performance comparison with FEM

Fig. 5 shows a composite structure consisting of three cubic blocks made of copper, G10 composite and stainless steel SS304. One side of the structure is kept at a fixed temperature (350 K) while the initial and the temperature at the other side is set at 300 K. All other wall have insulation boundary condition in both FEM and MCM simulations. Each cube has a side length equal to 0.01 m.

The temperature-dependent material properties shown in Fig. 6 are entered to both a finite element package (ANSYS) and used in the Monte-Carlo solver described in this paper. A transient heat conduction analysis with a time step equal to 0.02 s was done for a total time of 2 s. The number of nodes used in the FEM model was equal to the number of points in the Monte-Carlo simulation to make the comparison meaningful.

Fig. 7 shows the location of sources for two different sinks, each on the interface of two different materials in the composite structure. The sink on the interface between copper and G10 receives particles from farther distance in the copper, compared to the

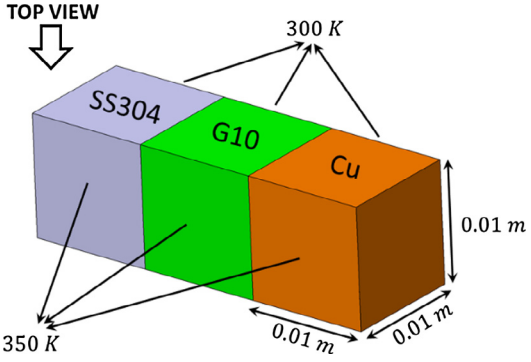

Fig. 5. Composite structure made of three materials.

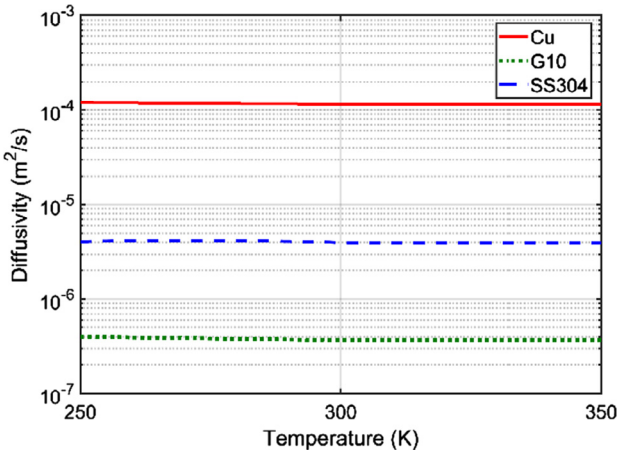

Fig. 6. Thermal diffusivity of materials used in the composite structure shown in Fig. 5 as function of temperature.

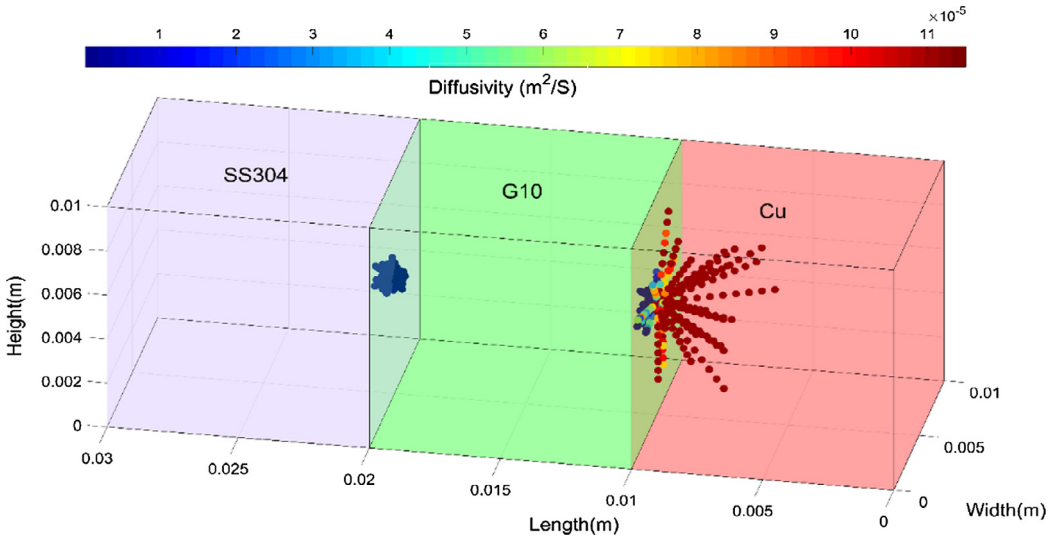

Fig. 7. Distribution of sources for two sinks located on interfaces of composite structure.

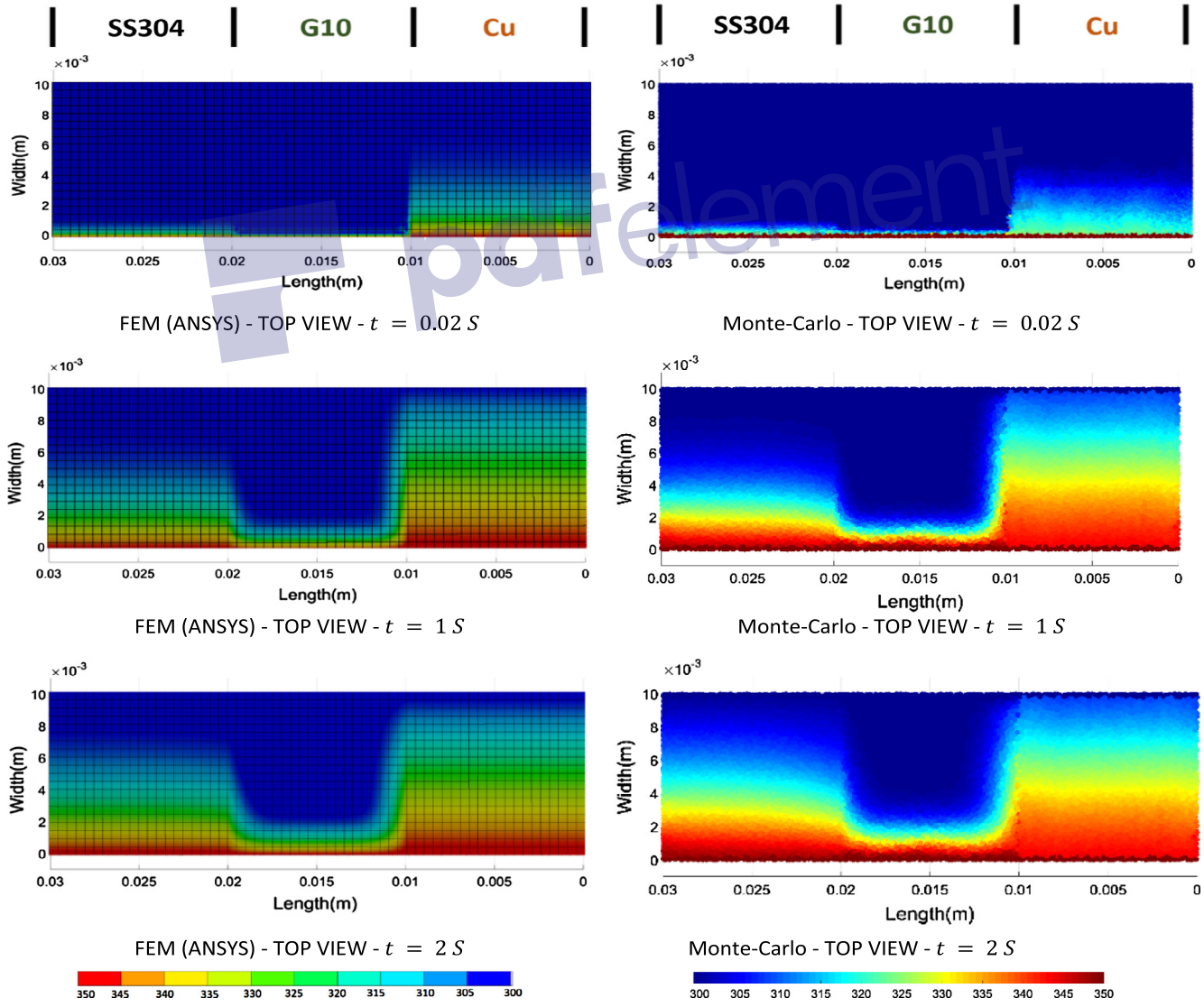

Fig. 8. Comparison of temperature distribution via MCM vs. FEM simulation, for three dimensional transient temperature propagation.

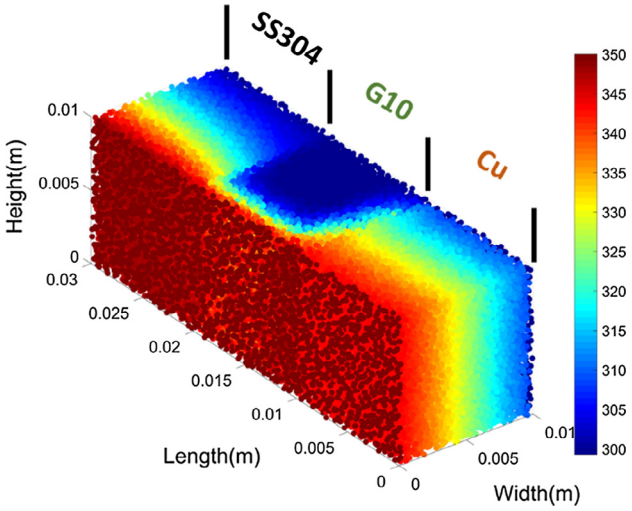

Fig. 9. Three-dimensional temperature distribution at t = 2 s.

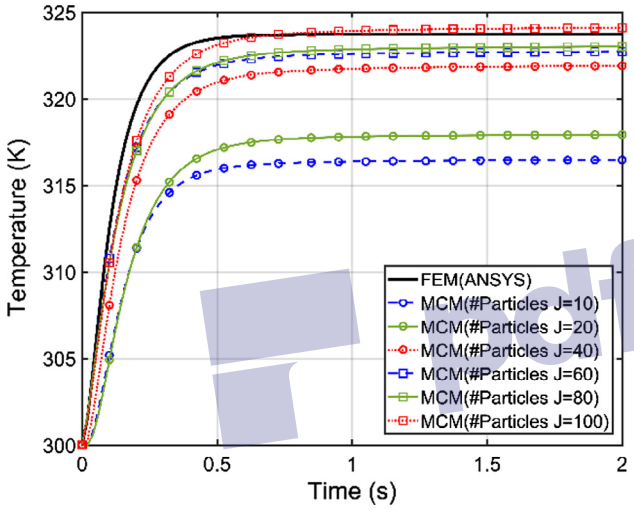

Fig. 10. Convergence of MCM and FEM for different numbers of particles at the middle point of the top of the copper block.

G10 side. This illustrates how the modified Eqs. (12) and (13) take thermal diffusivity of the path into account. The other sink, located on the interface between SS304 and G10 does not show substantial difference in steplengths as in the previous case – this reflects more similar values of thermal diffusivity for SS304 and G10 compared to the difference between Cu and G10.

Fig. 8 compares simulation results for MCM versus FEM at different times. There is good agreement between both methods, but the proposed MCM method is very well suited for parallelization and GPU computing, where transient analysis in FEM is not. The number of points used in the MCM simulation is equal to number of nodes in FEM ($K = 107$k, number of particles $J = 100$, and path length is divided by $M = 10$ substep lengths).

Fig. 9 shows the three dimensional temperature distribution in the composite structure at t = 2 s.

For a quantitative comparison between FEM and MCM in the above example, two points at the middle of the top surface were chosen (in m): $k_1 = (0.005, 0.005, 0.01)$ and $k_2 = (0.025, 0.005, 0.01)$, located at the copper and SS304 blocks, respectively. Fig. 10 shows the temperature at point k_1 and its convergence against number of particles in MCM compared to FEM. Fig. 11 shows the impact of number of particles in convergence for point k_2, located on the top surface of the stainless steel block (SS304). The number of points in MCM is equal to number of nodes

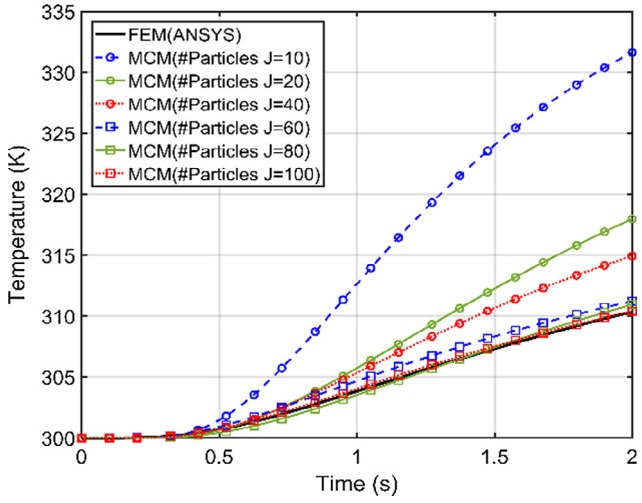

Fig. 11. Convergence of MCM to FEM versus number of particles at the middle point on the stainless steel block.

in FEM $K = 107$k; the number of particles emitted from each source vary from 10 to 100. This illustrates the convergence of MCM to FEM by increasing the number of particles; in this example $J = 100$ particles is enough to reach accurate results with less than one percent error.

4. Experimental verification

An experiment was designed to verify the simulation results presented in this paper. Fig. 12 shows the test article, in which a

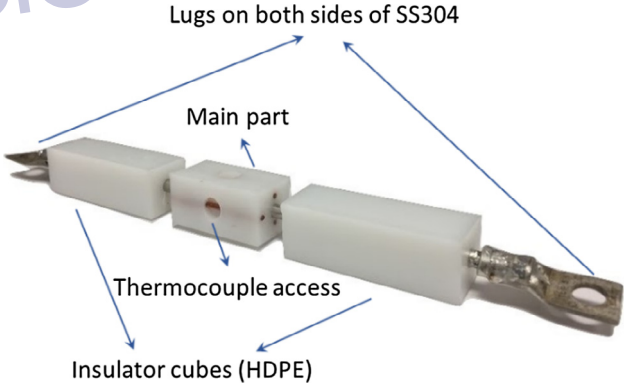

Fig. 12. Test article.

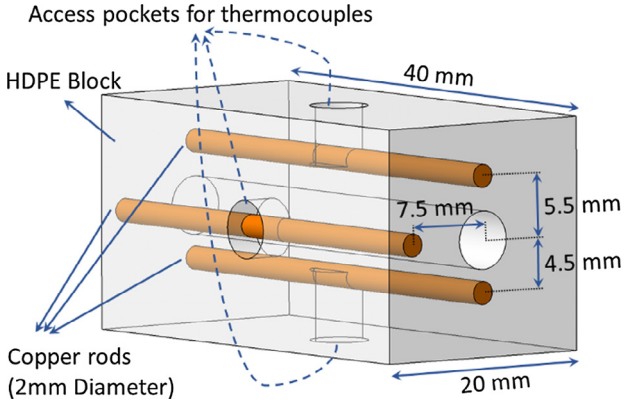

Fig. 13. Main component of the test article for 3D conductive heat transfer measurements.

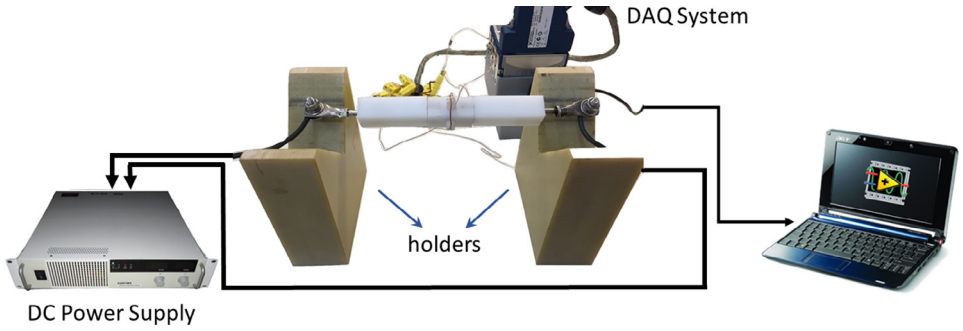

Fig. 14. Test setup and data acquisition system for experimental verification of MCM simulations.

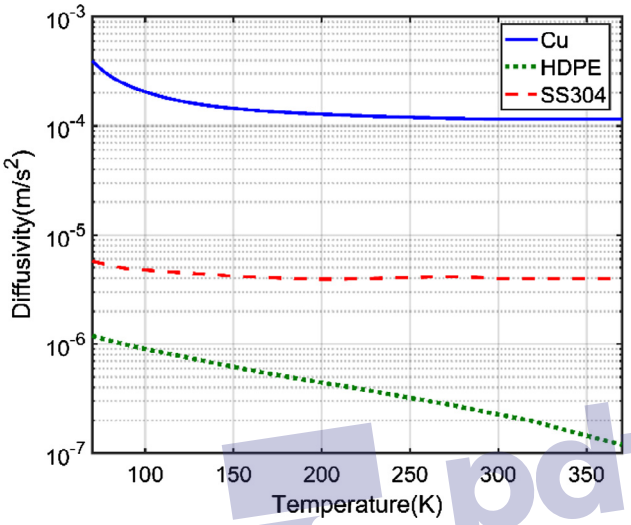

Fig. 15. Thermal diffusivity of materials used in the experimental verification, as function of temperature.

200 mm-long stainless steel rod of 5 mm diameter (SS304) is passed through three blocks of high-density polyethylene (HDPE). Both ends of the rod are attached to lugs filled with solder to ensure excellent electrical contact between rod and lugs. The middle block is the main component, where temperature measurements are acquired using embedded copper rods. Fig. 13 shows the layout of the main component. Three copper rods of 2 mm diameter are tightly embedded in the material through holes in the HDPE block to ensure excellent thermal contact. The axial distances from the center of each copper rod to the center of the stainless steel rod are 4.5 mm, 5.5 mm and 7.5 mm, as shown in Fig. 13. The cross section of the main component is a square of 20 mm length, and the height of the bock is 40 mm. Two HDPE blocks on either side of the main component act as thermal insulation to minimize the convective effect on the measurements.

Fig. 14 shows the complete experimental set up. Both insulator blocks are compressed against the main component to provide a tight contact. A DC power supply provides 70 A of DC current to the steel rod. A data acquisition system, NI 9214 set to its highest resolution (16-bit, or 0.15% error) is used to record the measured temperatures at a sample rate of 1 sample/s. Three thermocouples are used to read the temperatures of the copper rods, and one is used for the temperature of the stainless steel rod, as is heated up by the current provided by the power supply. All measured temperatures are recorded to a file using LabVIEW. A finite element model is implemented in ANSYS to compare with the results of the MCM simulation. Fig. 15 shows the material properties used in both the FEM and MCM simulations.

The measured temperature of the stainless steel rod is fed to the transient temperature profile of the rod in the middle of the main

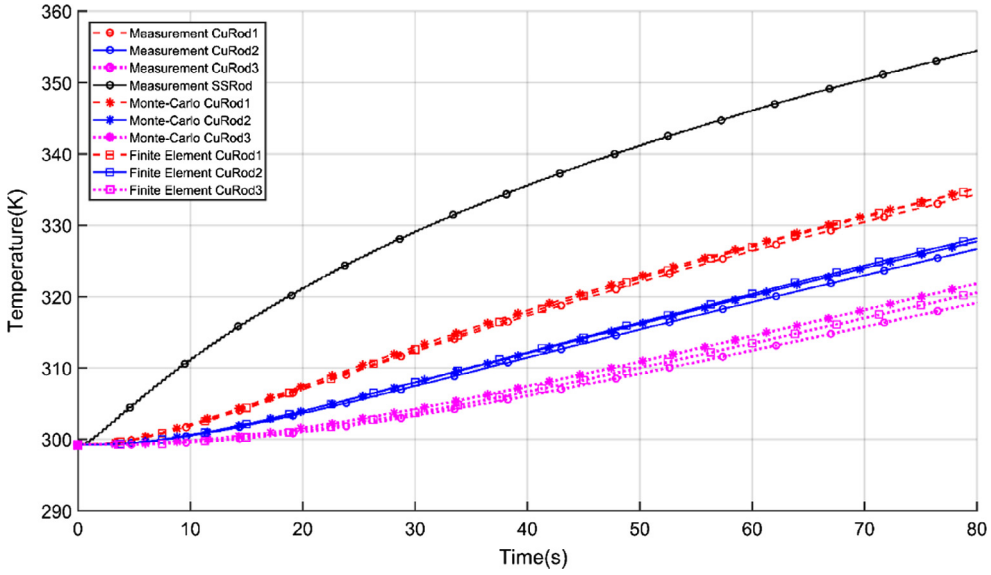

Fig. 16. Simulation results using the proposed Monte-Carlo method (MCM) for transient conductive heat transfer in composite materials with temperature dependent properties, compared with experimental measurements and FEM simulation.

block for both FEM and MCM simulations. The number of nodes in the FEM model is set equal to the number of points in the MCM simulation to provide comparable conditions. The transient simulations are done for t = 80 s. All external walls of the HDPE blocks are considered insulated in both FEM and MCM simulations, and the time step for both simulations is set as $t = 0.05$ s. The results of both simulations are shown in Fig. 16. The proposed Monte-Carlo approach leads to predictions of the transient temperature profiles that agree with both the measurements and FEM results. As time passes, a small divergence between measurements and both numerical methods is found, due to convective heat transfer affecting the measurements. The divergence is larger in the copper rods closer to the surface of the HDPE block, since the convective effect is more significant on them.

5. Conclusion

A novel three-dimensional Monte-Carlo method for the simulation of the transient conductive heat transfer in composite materials with temperature- dependent properties has been presented. The proposed method combines a transient Bessel function solution with a steady state peripheral integral method to simulate the transient heat conduction in composite materials with temperature dependent material properties. The proposed method is mesh-free, which makes it well suited for modeling complex geometries and multi-scale problems, where conventional FEM tools may lead to large number of elements and hence prohibitive simulation times. The proposed method converges to correct results, as verified by both experimental measurements and FEM simulations, with a relatively small number of required particles. This fact, along with its suitability for parallelization, makes it a very promising approach for the simulation of complex problems such as the multi-physics analysis of quench in superconducting magnets. Both first and second kinds of boundary conditions were developed and verified against FEM and measurements. The extension of the proposed approach to the third kind of boundary condition (convection) suggests a promising step for future development.

References

[1] L.J. Peltier, S. Biringen, A. Chait, Application of implicit numerical techniques to the solution of the three-dimensional diffusion equation, Numer. Heat Transf. Part B Fundam. 18 (2) (Oct. 1990) 205–219.

[2] R. Bahadori, H. Gutierrez, S. Manikonda, R. Meinke, Monte Carlo method simulation for two-dimensional heat transfer in homogenous medium and proposed application to quench propagation simulation, IEEE Trans. Appl. Supercond. 27 (4) (2017) 1–5.

[3] D. Netter, J. Leveque, P. Masson, A. Rezzoug, I. Terms, M. Carlo, Monte Carlo method for transient Eddy-Current calculations, IEEE Trans. Magn. 40 (5) (2004) 3450–3456.

[4] A. Haji-Sheikh, F. Buckingham, Multidimensional inverse heat conduction using the Monte Carlo method, ASME J. Heat Transf. 115 (1) (1993) 26–33.

[5] S. Shafiee, M.H. McCay, Different reactor and heat exchanger configurations for metal hydride hydrogen storage systems – a review, Int. J. Hydrogen Energy 41 (22) (2016) 9462–9470.

[6] S. Du, M.-J. Li, Q. Ren, Q. Liang, Y.-L. He, Pore-scale numerical simulation of fully coupled heat transfer process in porous volumetric solar receiver, Energy (2017).

[7] A. Kasaeian et al., Nanofluid flow and heat transfer in porous media: a review of the latest developments, Int. J. Heat Mass Transf. 107 (2017) 778–791.

[8] S. Shafiee, M.H. McCay, S. Kuravi, Effect of magnetic fields on thermal conductivity in a ferromagnetic packed bed, Exp. Therm Fluid Sci. 86 (2017) 160–167.

[9] M.H. Gharahcheshmeh et al., Superconducting transition width (ΔT_c) characteristics of 25 mol% Zr-added (Gd, Y)$Ba_2Cu_{3O7-\delta}$ superconductor tapes with high in-field critical current density at 30 K, Supercond. Sci. Technol. 30 (1) (Jan. 2017) 15016.

[10] N. Metropolis, S. Ulam, The Monte Carlo Method, J. Am. Stat. Assoc. 44 (247) (1949) 335–341.

[11] A. Haji-Sheikh, E.M. Sparrow, The floating random walk and its application to Monte Carlo solutions of heat equations*, SIAM J. Appl. Math. 14 (2) (1966) 370–389.

[12] F. Kowsary, S. Irano, Monte Carlo solution of transient heat conduction in anisotropic media, J. Thermophys. Heat Transf. 20 (2) (2006) 342–346.

[13] F. Kowsary, M. Arabi, Monte Carlo solution of anisotropic heat conduction, Int. Commun. Heat Mass Transfer 26 (8) (1999) 1163–1173.

[14] V. Sizyuk, A. Hassanein, Efficient Monte Carlo simulation of heat conduction problems for integrated multi-physics applications, Numer. Heat Transf. Part B Fundam. 66 (5) (2014) 381–396.

[15] S. Talebi, K. Gharehbash, H.R. Jalali, Study on random walk and its application to solution of heat conduction equation by Monte Carlo method, Prog. Nucl. Energy 96 (2017) 18–35.

[16] S.K. Fraley, T.J. Hoffman, P.N. Stevens, A Monte Carlo method of solving heat conduction problems, J. Heat Transf. 102 (February 1980) (1980) 121–125.

[17] H.S. Horatio, S. Carslaw, John C. Jaeger, Conduction of heat in solids. Clarendon Press, 1959.

[18] A. Haji-Sheikh, Application of Monte Carlo Methods to Thermal Conduction Problems, University of Minnesota, 1965.

[19] J.Y.M. W.J. Minkowycz, E.M. Sparrow, Handbook of Numerical Heat Transfer, Second Hoboken, New Jeresey: Wiley, 2006.

[20] L. Farnell, W.G. Gibson, Monte Carlo simulation of diffusion in a spatially nonhomogeneous medium: correction to the Gaussian steplength, J. Comput. Phys. 198 (1) (2004) 65–79.

[21] L. Farnell, W.G. Gibson, Monte Carlo simulation of diffusion in a spatially nonhomogeneous medium: a biased random walk on an asymmetrical lattice, J. Comput. Phys. 208 (1) (2005) 253–265.

[22] R. Bahadori, H. Gutierrez, S. Manikonda, R. Meinke, Two-dimensional transient heat conduction in multi-layered composite media with temperature dependent thermal diffusivity using floating random walk Monte-Carlo method, Int. J. Heat Mass Transf. 115 (2017) 570–580.

[23] L.C. Burmeister, The effect of space-dependent thermal conductivity on the steady central temperature of a cylinder, J. Heat Transfer 124 (1) (2001) 195–197.